PCCP

Accepted Manuscript

ROYAL SOCIETY OF CHEMISTRY

www.rsc.org/pccp

Computational Investigation of NH_3 Adsorption and Dehydrogenation on W-modified Fe(111) surface

Ming-Kai Hsiao,[1,a] Chia-Hao Su,[2,a] Ching-Yang Liu,[1] and Hui-Lung Chen[1,*]

[1] Department of Chemistry and Institute of Applied Chemistry, Chinese Culture University, Taipei, 111, Taiwan

[2] Center for Translational Research in Biomedical Sciences, Kaohsiung Chang Gung Memorial Hospital, Kaohsiung 833, Taiwan

Corresponding Author:

*Hui-Lung Chen: chl3@faculty.pccu.edu.tw

Telephone: +886-2-28610511 ext 25313

Fax: +886-2-28617006

Equally Contribution Note:

[a] Both authors contributed equally to this work

Abstract

The hydrogen gas plays an important role in the future application since it could replace for gasoline, heating oil, natural gas, and other fuels. In previous reported, the ammonia (NH_3) has a high hydrogen content, and provides a promising mode of the transferring and storing of hydrogen for its on-site generation. Therefore, the dehydrogenation of NH_3 on metal surface was studied widely in the several decades. In our study, we employed monolayer tungsten metal to modify Fe(111) surface, denoted as W@Fe(111), trying to calculate the adsorption and dehydrogenation behaviors of NH_3 on W@Fe(111) surface via the first-principles calculations based on density function theory (DFT). The three adsorption sites of the surface were considered, such as top (T), 3-fold-shallow (S), and 3-fold-deep (D) sites. The most stable structure of NH_x (x = 0–3) species on the surface of W@Fe(111) have been predicted. The calculated activation energies for NH_x (x = 1–3) dehydrogenations are 19.29 kcal/mol (for H_2N-H bond activation), 29.17 kcal/mol (for $HN-H$ bond activation) and 27.94 kcal/mol (for $N-H$ bond activation), respectively, and the entire process is exothermic by 33.05 kcal/mol. To gain detailed knowledge into the catalytic processes of the NH_3 molecule on W@Fe(111) surface, the physical insights between adsorbate/substrate interaction and interface morphology are subjected to a detailed electronic analysis.

1. Introduction.

During the past two decades, alternative energy resource become very important because of the decreased fuel oil product. As an environmentally benign replacement for fuel, the hydrogen energy has been attracted more and more attention in the world, because it is abundant, pollution-free, renewable.[1] Searching sources and carriers of clean hydrogen have received considerable attention in recent years. Scientist expects that the hydrogen energy would be widely employed in the future and replace oil fuel. So far, a huge amount of research has been performed regarding storage of hydrogen in a convenient and efficient. However, the conventional method of prepared hydrogen gas would lead to a large huge of CO_x as byproducts, which are the greenhouse gas as human known and bring many disastrous environmental effects. Therefore, carbon-free nature compounds become important. The ammonia is one of them and it is also pollution-free onboard. NH_3 molecule is one of the largest volume chemicals in the word and is already an infrastructure exists.[2-4] It has a high hydrogen content (17.7 wt.%), so NH_3 provides a promising mode of the transfer and stored of hydrogen for its on-site generation.[5-7] In recent years, ammonia catalytic dehydrogenation on the metal,[8-14] alloy,[15] metal oxides[16,17] has been an project of the most extensively investigation. Thus, the decomposed ammonia become great importance for the industry and economy.

The dehydrogenation mechanisms of NH_3 molecule on varied metal surfaces

have already been studied widely,[14,18,19] and the reaction processes consists of the following four steps: $NH_{3(g)} \rightarrow NH_{3(a)}$, $NH_{3(a)} \rightarrow NH_{2(a)} + H_{(a)}$, $NH_{2(a)} \rightarrow NH_{(a)} + H_{(a)}$, $NH_{(a)} \rightarrow N_{(a)} + H_{(a)}$, $N_{(a)} + N_{(a)} \rightarrow N_{2(g)}$, and $H_{(a)} + H_{(a)} \rightarrow H_{2(g)}$, where the subscripts (g) and (a) denote the gas-phase and absorbed state, respectively. In the previous report, the calculated results showed the second step dehydrogenation process is the rate-determining step (RDS) for NH_3 dehydrogenation on the single-crystal metal surfaces.[9,20,21] Previously, we have studied the adsorption and dehydrogenation of the NH_3 molecule on Fe(111) and W(111) surfaces by employing the DFT approach, and it was found that the adsorption ability of NH_3 on W(111) are generally more stable than that of Fe(111) counterpart by ca. 6.25 kcal/mol.[21,22] Besides, the energy barrier for the first dehydrogenation process in NH_3/W(111) is slightly lower than NH_3/Fe(111) by ca. 0.7 kcal/mol, and it will turn to be ca. 4.2 and 2.5 kcal/mol higher for the second and third dehydrogenation processes.

Therefore, we want to modify the Fe(111) surface via coating monolayer with several tungsten metals. We performed DFT calculation to investigate NH_3 dehydrogenation on this modified system, denoted as W@Fe(111), to shed light on individual bonding and cleavage processes. The adsorption geometries/energies, site preference, relative stability of NH_3 and its dehydrogenated species, as well as activation barriers were systematically characterized. We believe that this

understanding is essential in the future study to rationally design of the catalytic surface model in the dehydrogenation of NH_3 molecule.

2. Computational Methods.

The electronic structure calculations were based on periodic density function theory (DFT) as implemented in Vienna ab initio Simulation Package (VASP).[23-27] The electron-ion interaction were carried out via projector augmented wave (PAW) method,[28,29] and the exchange-correlation effects were describe with Generalized Gradient Approximation with revised Perdew-Burke-Ernzerhof (GGA-rPBE).[30,31] The electronic state were expanded by using plane wave basis set with cut-off energy 400 eV, which allows convergence to 1×10^{-4} eV in total energy. The Brillouin zone is sampled with the Monkhorst-pack grid.[32] The calculations were performed with the (4 × 4 × 4) and (4 × 4 × 1) Monkhorst-Pack mesh *k*-points for bulk and surface calculations, respectively. All calculations were carried out by using the spin-polarization method to describe the magnetic property of the W@Fe(111) surface model properly. The p(3 × 3) lateral cell of W@Fe(111) surface is modeled as periodically repeated slabs with six layers, as shown in Figure 1(a). The bottom three atomic layers were kept frozen and set to the estimated bulk parameter, whereas the remaining layers were fully relaxed during the calculations. We performed

calculations for NH_3 and its fragments NH_x adsorbing on (3×3) surface, corresponding to coverage 1/9 ML. The lateral cell has dimensions of a = b =12.01 Å and c = 18.94 Å, which includes a vacuum region of thickness greater than 15 Å to ensure no interaction between the slabs. In this work, we calculate adsorption energies according to the following equation:

$$E_{adsorption} = E_{adsorbate-surface} - (E_{surface} + E_{gas\text{-}phase\ molecule})$$

Where $E_{adsorbate-surface}$, $E_{surface}$, and $E_{gas\text{-}phase\ molecule}$ are the calculated electronic energies of adsorbed species on the W@Fe(111) surface, a clean W@Fe(111) surface, and a gas-phase molecule, respectively. A negative value of $E_{adsorption}$ indicates an exothermic adsorption process. Vibrational frequencies of the adsorbed structures were analyzed by diagonalizing the hessian matrix of selected atoms within the VASP approach. The nudged-elastic-band (NEB) method[33-35] was applied to locate transition structures, and minimum energy pathways (MEP) were constructed accordingly.

3. Results and Discussion.

Previously, Chen et al.[36] calculated the lattice parameters of bulk Fe via rPBE functional (with the consideration of spin polarization) and found its lattice constant, 2.836 Å, which approaches the experimental value 2.866 Å. They also studied the magnetic moment of the bulk Fe, 2.23 μ_B, agreeing satisfactorily with the

experimental value, 2.22 μ_B. On the other hand, the lattice parameters of bulk W at rPBE functional have also been reported by Chen et al.,[37] and the result shows 3.181 Å, which is closely with the experimental value of 3.165 Å. Their calculated results also showed that the bond lengths are within the 2.750~2.754 Å between neighboring W metals, which is also in satisfactory agreement with experimental value, 2.741 Å. In addition, the structures, frequencies and bond energies of the isolated gas-phase molecule, NH_3, and its fragments, NH_2 and NH, are examined in a large unit cell of 25 × 25 × 25 $Å^3$ dimensions with rPBE functional. All these calculated data were fully compared with experimental properties, showing a good agreement with the experimental values.[22] Therefore, in this work we are confident in the reliability of the following simulated results by rPBE functional for NH_3/W@Fe(111) system.

For exploring the dehydrogenation process of NH_3 onto the W@Fe(111) surface, we studied the optimized adsorption geometries and energies of the NH_3, as well as its fragments, which are symbolized as NH_3/W@Fe(111), NH_2/W@Fe(111), NH/W@Fe(111), N/W@Fe(111) and H/W@Fe(111), respectively. To examine the site preference of adsorption for W@Fe(111) surface, each fragment have been placed in every possible locations. Three typical adsorption sites were considered, such as the top (T), 3-fold-shallow (S), and 3-fold-deep (D), as shown in Figure 1. For the top site (T), the molecule adsorbs on the top of the first-layer W metal of W@Fe(111). At the

3-fold-shallow site (S), the molecule coordinates above the second-layer Fe metal. At the 3-fold-deep site (D), the molecule adsorbs above the third-layer Fe metal.

As shown in Table 1, we found several more stable isomers of NH_3 adsorbed on W@Fe(111) surface. Those structures (shown in Figure 2) are classified according to the adsorption sites which are denoted as follows: W@FeNH_3(T-η^1-N)-a, W@FeNH_3(T-η^1-N)-b, W@FeNH_3(T,T-μ^2-N)-a and W@FeNH_3(T,T-μ^2-N)-b, with the adsorption energies of -22.09, -21.99, -17.08, and -16.82 kcal/mol, respectively. Apparently, the energetically most stable structure is the adsorption at the top site via the N atom of NH_3, and its three H atoms in the direction above the deep sites. As compared to previous theoretical studies of ammonia adsorption on other transition metal surfaces,[21,38-40] it is found that these computed results also reflected similar location of adsorption with our simulated outcomes. Among our preferred adsorbed geometries of W@FeNH_3(T-η^1-N)-a and W@FeNH_3(T-η^1-N)-b, the distances between the nitrogen atom and the surface are about 2.248~2.264 Å and the N-H bond lengths of adsorbed NH_3 are within the range of 1.023~1.024 Å, which are close to the values of the isolated molecule (1.017 Å).[41] Besides. the cone angles of H-N-H are slightly increased to 108.8~109.0° as compared to gas-phase NH_3 (107.8°).[41] As a result, it is obvious that the configuration of the adsorbed NH_3 is not seriously distorted by W@Fe(111) surface.

In addition, adsorbed NH_2 was calculated to have three more stable isomers on W@Fe(111) surface, which are represented by W@$FeNH_2$(T-η^1-N), W@$FeNH_2$(T,T-μ_2-N), and W@$FeNH_2$(T,S-μ_2-N) with the adsorption energies of -80.99, -73.07, and -68.20 kcal/mol, respectively. The important geometrical parameters and adsorption energies are also tabulated in Table 1. As shown in Figure 3, the NH_2 favors to adsorb at the top site with the molecular C_2-axis perpendicular to W@Fe(111) and the two hydrogen atoms pointing to the deep and shallow site, accordingly. Any attempt to find a minimum of energy in the other symmetric site leads to the top site after complete optimization, which is in agreement with the published theoretical works of NH_2 adsorption on transition metals.[21,22] For the geometry of W@$FeNH_2$(T-η^1-N) with the highest adsorption energy, it is found that the bond length of N-W would dramatically decrease to 1.967 Å as compared to its original counterpart of NH_3 adsorption (W@$FeNH_3$(T-η^1-N)-a, 2.248 Å). The bond length of N-H and H-N-H bond angle are 1.018/1.019 Å and 110.5°, respectively, which are close to those of isolated NH_2 in gas-phase (1.024 and 103.4°).[41] While for NH fragment, three adsorbed isomers were found in our calculations, which were denoted by W@FeNH(T,T,S-μ_3-N), W@FeNH(T,T-μ_2-N), and W@FeNH(T,T,T-μ_3-N), respectively. Among them, the NH fragment preferred to form the tridenate construction, W@FeNH(T,T,S-μ_3-N), with the adsorption energy of -115.87 kcal/mol,

which is better than another possible sites by ca. 0.3 ~ 3.0 kcal/mol. For this preferable adsorption structure, the bond length of N-H would decrease to 1.033 Å as compared to 1.038 Å in the gas-phase.[42] The distance of N-W is ca. 2.03 ~ 2.12 Å, which is slightly longer than NH_2/W@Fe(111) counterpart (1.967 Å).

Finally, we also investigated the adsorption of N and H atoms on W@Fe(111), and the calculated results are shown in Table 2. As shown in Figure 4, the N atom adsorbing on W@Fe(111) could lead to three different isomers: W@FeN(S-η^1-N), W@FeN(T,T,T-μ_3-N), and W@FeN(T,T,S-μ_3-N). As the results, the radical adsorbate N atom could adsorb strongly on W@Fe(111) surface, and the most favorable adsorption site is W@FeN(T,T,T-μ_3-N) with the adsorption energies of -144.23 kcal/mol. In addition, there are three stable adsorption isomers of H atom on W@Fe(111) surface, denoted as W@FeH(T-η^1-H), W@FeH(T,T,S-μ_3-H), and W@FeH(S-η^1-H), respectively. Among these kinds of adsorptions, the H radical favored to adsorb on the top site, W@FeH(T-η^1-H), with the adsorption energy of -59.95 kcal/mol.

The dehydrogenation mechanisms of NH_3 on a transition metal are commonly accepted as follows: [14,18,19]

$$NH_{3(g)} + S \rightarrow NH_{3(a)} \qquad \text{(i)}$$

$$NH_{3(a)} \rightarrow NH_{2(a)} + H_{(a)} \qquad \text{(ii)}$$

$NH_{2(a)} \rightarrow NH_{(a)} + H_{(a)}$ (iii)

$NH_{(a)} \rightarrow N_{(a)} + H_{(a)}$ (iv)

where S indicates the catalytic metal surfaces.

The potential energy diagram (shown in Figure 5) of NH_3 dehydrogenation process was mapping by NEB method, and their important geometrical parameters of intermediates, transition structures and product of the reaction are presented in Figure 6. For the discussion of dehydrogenation mechanism, since the energetically most stable configuration of NH_3/W@Fe(111) is W@FeNH_3(T-η^1-N)-a we explored the reaction path starting from it and denoted as **LM1**. The first dehydrogenation of NH_3 from **LM1** into adsorbed NH_2 and H producing **LM2** requires a activation barrier of 19.29 kcal/mol (**TS1**) with an exothermicity of 10.15 kcal/mol. At the transition state **TS1**, an imaginary frequency *i*606.5 cm^{-1} corresponding to the N-H stretching vibration mode was observed, and the distance of N-H bond for this dehydrogenation is around 1.285 Å. In **LM2**, both the co-adsorbed NH_2 and H are on the top sites. We then calculated the next transition state **TS2**, for **LM2** to form **LM3** directly, but this process involves a greater energy barrier (29.17 kcal/mol) and endothermic by 8.71 kcal/mol. In **LM3** (see Figure 6), the adsorbed NH fragment is on the top site position, which is less stable from our calculated result. The NH fragment can thus easily diffuse to the more stable site (between top and shallow) forming another

NH/2H/W@Fe(111) configuration, **LM4**. This process is found to be 6.88 kcal/mol exothermic and occurs with a small energy barrier (ca. 11.1 kcal/mol) at transition structure **TS3**. Finally, the **LM4** intermediate overcomes an activation barrier 27.94 kcal/mol at **TS4** to break the third N–H bond and produce **P**, N/3H/W@Fe(111), with an exothermicity 2.64 kcal/mol, in which the N atom is located between top and shallow and the H atoms were adsorbed on top sites. In order to obtain the minimum-energy pathway of above mechanism, it should be mentioned that we have already assumed the N and H atoms could easily diffuse and occupy to their preferable sites (with the higher adsorption energies) after dehydrogenation since the energy barriers of N and H migrations are quite low (within the range of ca. 1.0~3.0 kcal/mol). For the final desorption processes, such as association reactions of $H_{(a)}$ + $H_{(a)}$ → $H_{2(g)}$ and $N_{(a)}$ + $N_{(a)}$ → $N_{2(g)}$, are expected to be operated by a large entropy term at elevated temperature. One can hence trust that this endothermic character for the final step desorption would be easily achieved without further substantial efforts. Based on the aforementioned PES for the dehydrogenation of NH_3 on W@Fe(111), we proposed the dehydrogenation mechanism will be $NH_{3(g)}$ + W@Fe(111)→**LM1→TS1→LM2→TS2→LM3→TS3→LM4→TS4→P** and totally exothermic by 33.05 kcal/mol with respect to the reactants.

Among all NH_x dehydrogenation processes, the dehydrogenation of NH_2 is the

highest barrier. If the thermal energy could overcome the energy barrier of **TS2** (E_a = 29.17 kcal/mol), then all of the NH_x dehydrogenation processes could take place on the surface of W@Fe(111). Even though this activation energy of **TS2** on the W@Fe(111) surface is somewhat high, it is still lower than those for NH_3 dehydrogenations on Pt,[9] Rh[20] and W[22] surfaces, where the rate determining activation energies of the reactions on those metal surfaces range from ca. 31.3 to 37.1 kcal/mol. Similar smaller activation barrier of **TS2** was also found for Fe(111) surface (ca. 28.5 kcal/mol),[21] but the energy barrier for the first dehydrogenation processes in NH_3/W@Fe(111) is apparently lower than NH_3/Fe(111) by ca. 9.0 kcal/mol and the adsorption ability of NH_3 on W@Fe(111) are generally more stable than that of Fe(111) counterpart by ca. 5.8 kcal/mol. As a consequence, according to our present calculations and a lot of comparisons with other similar works, we could conclude that the W-modified Fe(111) surface exhibits a larger catalytic activity to decompose NH_3.

Figure 7 shows plots of the contour surface of the charge-density difference, $\Delta\rho_{diff} = \rho$[surface + adsorbate] – ρ[surface] – ρ[adsorbate], for each adsorbate/substrate system in the NH_3 dehydrogenation path: (a) before adsorption, (b) **LM1**, (c) **LM2**, (d) **LM4**, (e) **P**, respectively. In addition, we analyze the DFT electron density of the aforementioned adsorbed intermediates and product (see in

Figure 6 for number labeling) with Bader's method.[43,44] From the Figure 7a to 7b, the charge transferred between NH_3 molecule (through first layer) and W@Fe(111) surface is very small (only 0.02 |e|, from W metals to NH_3). As the first dehydrogenation proceeds, 0.76 electron is transferred from the W@Fe(111) surface to the NH_2 fragment (see Figure 7c, **LM2**). In the second and third dehydrogenation processes, the phenomena of charge transfer become much severe. This value increases to 1.35 and 2.13 electron for **LM4** (from W@Fe(111) to the NH fragment, Figure 7d) and **P** (from W@Fe(111) to the N atom, Figure 7e), respectively. As a consequence, one can hence forecast that a extraordinary transfer of charge between the adsorbate and the substrate will play a significant role in accelerating the catalytic processes for NH_3 dehydrogenation.

Furthermore, to be more distinct, we investigated the electronic local density of states (LDOS) of the system projected on the orbitals for the adsorbate, nitrogen and hydrogen species, as well as the W@Fe(111) substrate (shown in Figure 8). The degree of hybridizing between adsorbate and substrate electronic state would provide us another evidence to realize the adsorption and dehydrogenation behaviors. Figure 8a shows the LDOS before the NH_3 adsorbed on the W@Fe(111). Figures 8b-8e correspond to the LDOS of **LM1**, **LM2**, **LM4** and **P** configurations, respectively. In addition, as it is well-known that the electronic structure of NH_3 in the gas phase can

be represented as $\left(\sigma_{2a_1}\right)^2\left(\sigma_{1e}\right)^4\left(n_{3a_1}\right)^2$, where σ_{1e} included two degenerated orbitals. Therefore, we could observe that there are three distinct peaks shown in Figure 8a along the energy scale from the -15.0 eV to 0.0 eV representing σ_{2a_1}, σ_{1e}, and n_{3a_1} orbitals, respectively. Upon adsorption, the peaks below the Femi level (see Figure 8b) are with extraordinary downward shifts, especially the third peak is with a distinct downward shift and height decreasing, suggestive of the substantial interaction between the d-band of the W metals and the three states of NH_3 which could lead to a charge transfer from W metals to NH_3 molecule. As the dehydrogenations proceed (see from Figure 8c to 8e), the stronger hybridization behaviors between the N (or H) atom (*p* or *s* orbitals) and W@Fe(111) surface (*d* orbital) were found (particular states vanished unexpectedly and turned into broad in a range of -10.0 ~ -2.5 eV). It is also found that the stronger hybridization phenomenon was observed in Figure 8e, indicating that the noteworthy states coupling and pronounced broadening (much stronger hybridization) happened at the final dissociative stage. The aforementioned results provide a rational explanations of the larger molecular adsorption energy and obviously mutual interaction between the adsorbate and the bimetallic substrate.

4. Conclusion

The dehydrogenation behaviors of NH_3 on bimetallic surface of W@Fe(111)

have been analyzed with periodic DFT calculations. The possible adsorption sites, geometrical parameters, and adsorption energies of the NH_3 and its fragments on W@Fe(111) surface are presented. The calculated results show that the adsorbed isomers of W@$FeNH_3$(T-η^1-N)-a, W@$FeNH_2$(T-η^1-N), W@FeNH(T,T,S-μ_3-N), W@FeN(T,T,T-μ_3-N), and W@FeH(T-η^1-H), are energetically favorable among all calculated structures of NH_3/W@Fe(111), NH_2/W@Fe(111), NH/W@Fe(111), X/W@Fe(111) (where X = N and H atoms), respectively. In our predicted catalytic process, it is found that the NH_3 dehydrogenations are via four-step mechanism, which agrees satisfactorily with experimental predictions, and the entire process is exothermic by -33.05 kcal/mol with respect to the reactants. It should be mentioned that the activation barrier of the first dehydrogenation is slightly lower than that of desorption energy for NH_3 on W@Fe(111) surface by 2.8 kcal/mol. The competing reaction, however, between the first dehydrogenation and desorption phenomenon could be controlled in condition of the applied pressure and temperature. All the information predicted by theoretical approaches would be difficult to accomplish with experimental measurements, indicative of the periodic DFT calculations could play a important role in the prospective design of high-performance catalytic surfaces for the dehydrogenation of NH_3.

Acknowledgment

H.-L.C. would like to acknowledge (1) the National Science Council, Republic of China, under Grant No. MOST 104-2113-M-034-002 for financial supports, (2) the Taiwan Ministry of Science and Technology, Republic of China, under Grant No. MOST 102-2113-M-034-002-MY2, MOST 103-2633-B-182A-001- (C.-H. S.), and MOST103-2320-B-182A-004-MY3 (C.-H. S) for financial supports, (3) financial supports by the Chinese Culture University, and (4) the National Center for High-Performance Computing, Taiwan, for the use of computer time.

References

1 Z. Jiang, Q. Pan, M. Li, T. Yan and T. Fang, *Appl. Surf. Sci.*, 2014, **292**, 494-499.

2 T. V. Choudhary, A. K. Santra, C. Sivadinarayana, B. K. Min, C. W. Yi, K. Davis and D. W. Goodman, *Catal. Lett.*, 2001, **77**, 1-5.

3 T. V. Choudhary, C. Sivadinarayana and D. W. Goodman, *Catal. Lett.*, 2001, **72**, 197-201.

4 A. K. Santra, B. K. Min, C. W. Yi, K. Luo, T. V. Choudhary and D. W. Goodman, *J. Phys. Chem. B*, 2002, **106**, 340-344.

5 M. R. Rahimpour and A. Asgari, *Int. J. Hydrogen Energ.*, 2009, **34**, 5795-5802.

6 M. Diwan, D. Hanna and A. Varma, *Int. J. Hydrogen Energ.*, 2010, **35**, 577-584.

7 L. Li and J. A. Hurley, *Int. J. Hydrogen Energ.*, 2007, **32**, 6-10.

8 R. Imbihl, R. J. Behm and R. Schlogl, *Phys. Chem. Chem. Phys.*, 2007, **9**, 3459-3459.

9 C. Popa, W. K. Offermans, R. A. van Santen and A. P. J. Jansen, *Phys. Rev. B*, 2006, **74**, 155428.

10 G. Novell-Leruth, A. Valcarcel, A. Clotet, J. M. Ricart and J. Perez-Ramirez, *J. Phys. Chem. B*, 2005, **109**, 18061-18069.

11 G. Novell-Leruth, A. Valcarcel, J. Perez-Ramirez and J. M. Ricart, *J. Phys. Chem. C*, 2007, **111**, 860-868.

12 E. Herceg, K. Mudiyanselage and M. Trenary, *J. Phys. Chem. B*, 2005, **109**, 2828-2835.

13 W. Huang, W. Lai and D. Xie, *Surf. Sci.*, 2008, **602**, 1288-1294.

14 G. Lanzani and K. Laasonen, *Int. J. Hydrogen Energ.*, 2010, **35**, 6571-6577.

15 E. Moran, C. Cattaneo, H. Mishima, B. A. L. de Mishima, S. P. Silvetti, J. L. Rodriguez and E. Pastor, *J. Solid State Electrochem.*, 2008, **12**, 583-589.

16 P. R. McGill and H. Idriss, *Langmuir*, 2008, **24**, 97-104.

17 C.-C. Wang, Y.-J. Yang and J.-C. Jiang, *J. Phys. Chem. C*, 2009, **113**, 2816-2821.

18 J. J. Mortensen, M. V. Ganduglia-Pirovano, L. B. Hansen, B. Hammer, P. Stoltze and J. K. Norskov, *Surf. Sci.*, 1999, **422**, 8-16.

19 A. Hellman, K. Honkala, I. N. Remediakis, A. Logadottir, A. Carlsson, S. Dahl, C. H. Christensen and J. K. Norskov, *Surf. Sci.*, 2009, **603**, 1731-1739.

20 W. K. Offermans, A. P. J. Jansen, R. A. van Santen, G. Novell-Leruth, J. M. Ricart and J. Perez-Ramirez, *J. Phys. Chem. C*, 2007, **111**, 17551-17557.

21 R.-J. Lin, F.-Y. Li and H.-L. Chen, *J. Phys. Chem. C*, 2011, **115**, 521-528.

22 M.-K. Hsiao, S.-K. Wu and H.-L. Chen, *J. Phys. Chem. C*, 2015, **119**, 4188-4198.

23 G. Kresse and J. Hafner, *Phys. Rev. B*, 1993, **47**, 558-561.

24 G. Kresse and J. Hafner, *J. Phys.-Condens. Mat*, 1994, **6**, 8245-8257.

25 G. Kresse and J. Hafner, *Phys. Rev. B*, 1994, **49**, 14251-14269.

26 G. Kresse and J. Furthmuller, *Phys. Rev. B*, 1996, **54**, 11169-11186.

27 G. Kresse and J. Furthmuller, *Comp. Mater. Sci.*, 1996, **6**, 15-50.

28 P. E. Blochl, *Phys. Rev. B*, 1994, **50**, 17953-17979.

29 G. Kresse and D. Joubert, *Phys. Rev. B*, 1999, **59**, 1758-1775.

30 J. P. Perdew, K. Burke and M. Ernzerhof, *Phys. Rev. Lett.*, 1996, **77**, 3865-3868.

31 Y. K. Zhang and W. T. Yang, *Phys. Rev. Lett.*, 1998, **80**, 890-890.

32 H. J. Monkhorst and J. D. Pack, *Phys. Rev. B*, 1976, **13**, 5188-5192.

33 A. Ulitsky and R. Elber, *J. Chem. Phys.*, 1990, **92**, 1510-1511.

34 G. Mills, H. Jonsson and G. K. Schenter, *Surf. Sci.*, 1995, **324**, 305-337.

35 G. Henkelman, B. P. Uberuaga and H. Jonsson, *J. Chem. Phys.*, 2000, **113**, 9901-9904.

36 H.-L. Chen, H.-T. Chen and J.-J. Ho, *Langmuir*, 2010, **26**, 775-781.

37 H.-T. Chen, D. G. Musaev and M. C. Lin, *J. Phys. Chem. C*, 2007, **111**, 17333-17339.

38 S. Stolbov and T. S. Rahman, *J. Chem. Phys.*, 2005, **123**, 204716.

39 F. Frechard, R. A. van Santen, A. Siokou, J. W. Niemantsverdriet and J. Hafner, *J. Chem. Phys.*, 1999, **111**, 8124-8130.

40 Y. Zhang, X. Xiao, Y. Cao, Y. Cai and J. Wang, *Int. J. Hydrogen Energ.*, 2013, **38**, 2965-2972.

41 G. Herzberg, *Molecular Spectra and Molecular Structure. Iii.: Electronic Spectra and Electronic Structure of Polyatomic Molecules*, Van Nostrand Reinhold Co., New York, 1966.

42 G. Herzberg, *Molecular Spectra and Molecular Structure Iv.; Constants of Diatomic Molecules;* , Van Nostrand Reinhold Co., New York,, 1979.

43 R. F. W. Bader and P. M. Beddall, *J. Chem. Phys.*, 1972, **56**, 3320-&.

44 R. F. W. Bader, *Atoms in Molecules : A Quantum Theory*, Clarendon Press, New York, 1990.

Table 1. Calculated adsorption energies (kcal/mol), and geometrical parameters (Å) of adsorbed NH_3, NH_2 and NH molecules on W@Fe(111) surface.

adsorption site	adsorption energy	d(W-N)[a]	d(N-H)[b]
For NH_3 molecule			
W@FeNH_3(T-η^1-N)-a	-22.09	2.264	1.023/1.024/1.024
W@FeNH_3(T-η^1-N)-b	-21.99	2.248	1.023/1.023/1.024
W@FeNH_3(T,T-μ_2-N,H)-a	-17.08	2.343	1.019/1.020/1.035
W@FeNH_3(T,T-μ_2-N,H)-b	-16.82	2.344	1.025/1.031/1.031
For NH_2 molecule			
W@FeNH_2(T-η^1-N)	-80.99	1.967	1.018/1.019
W@FeNH_2(T,T-μ_2-N)	-73.07	2.246	1.023/1.026
W@FeNH_2(T,S-μ_2-N)	-68.20	2.082	1.023/1.024
For NH molecule			
W@FeNH(T,T,S-μ_3-N)	-115.87	2.031	1.033
W@FeNH(T,T-μ_2-N)	-115.58	2.114	1.034
W@FeNH(T,T,T-μ_3-N)	-112.91	2.159	1.029

[a]The shortest distance between the adsorbed atom (N) and the corresponding adsorption sites of W metals.

[b]The bond lengths of NH^1 / NH^2 / NH^3 are presented.

Table 2. Calculated adsorption energies (kcal/mol) and geometrical parameters (Å) of adsorbed N and H atoms on W@Fe(111) surface.

adsorption site	adsorption energy	d(W-N or H)[a]
For N atom		
W@FeN(S-η^1-N)	-139.79	1.926
W@FeN(T,T,T-μ_3-N)	-144.23	2.032
W@FeN(T,T,S-μ_3-N)	-143.94	1.946
For H atom		
W@FeH(T-η^1-H)	-59.95	1.600
W@FeH(T,T,S-μ_3-H)	-58.29	1.645
W@FeH(S-η^1-H)	-57.81	1.623

[a]The shortest distance between the adsorbed atoms (N or H) and the corresponding adsorption sites of W metals.

Figure Captions

Figure 1. Schematic presentation of W@Fe(111) surface used in the present studies:(a) side view, and (b) top view. The **T**, **D** and **S** represent top, deep, and shallow sites. The first layer is tungsten metal and bottom five atomic layers is iron.

Figure 2. Located isomers of adsorbed NH_3 on W@Fe(111) surface and their important geometry parameters calculated at the rPBE level of theory. The bond lengths are given in angstroms.

Figure 3. Located isomers of adsorbed NH_2 and NH on W@Fe(111) surface and their important geometry parameters calculated at the rPBE level of theory. The bond lengths are given in angstroms.

Figure 4. Located isomers of adsorbed N and H on W@Fe(111) surface and their important geometric parameters calculated at the rPBE level of theory. The bond lengths are given in angstroms.

Figure 5. Calculated possible potential energy diagram for the dehydrogenation of NH_3 on the surface of W@Fe(111), where the numbers are the energies in kcal/mol and v_i represents the imaginary frequency of that particular transition state.

Figure 6. Geometrical illustration of intermediates, transition states, and products for the NH_3-W@Fe(111) interactions using the rPBE level of theory.

Figure 7. Illustration of charge-density difference for NH_3 dehydrogenation on W@Fe(111) via the proposed minimum-energy pathway: (a) before adsorption, (b) **LM1**, (c) **LM2**, (d) **LM4**, (e) **P**. The charge-density difference is calculated by using $\Delta\rho_{diff} = \rho[\text{surface + adsorbate}] - \rho[\text{surface}] - \rho[\text{adsorbate}]$. The values are effective charges which are calculated by Bader analysis program.

Figure 8. Local density of states (LDOS) for NH_3 dehydrogenation on W@Fe(111) along the proposed minimum-energy pathway: (a) before interaction, (b) **LM1**, (c) **LM2**, (d) **LM4**, and (e) **P**. The black, red and blue lines represent W@Fe(*d*), N(*p*) and H(s), respectively. The dashed line represents the Fermi level.

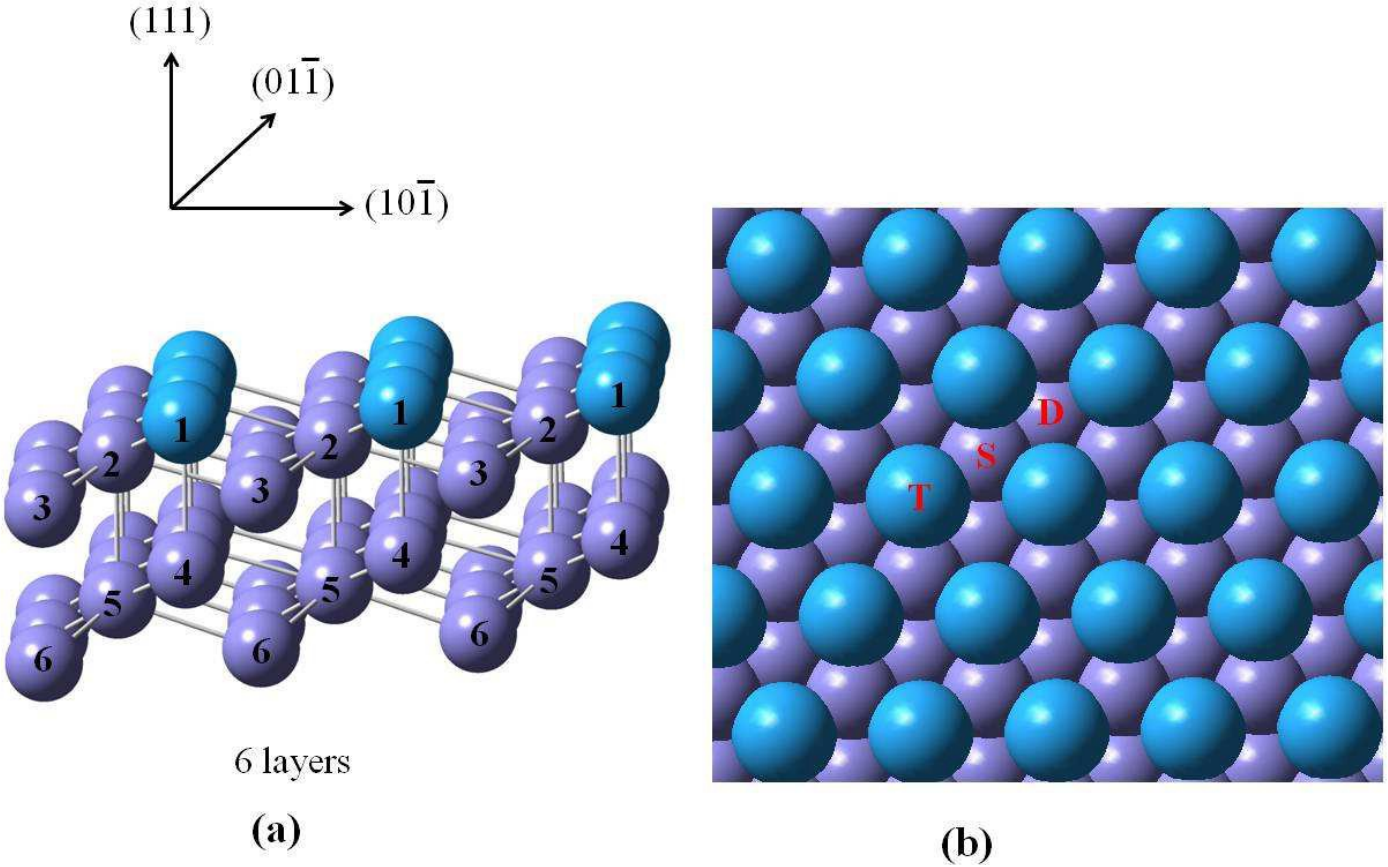

Figure 1.

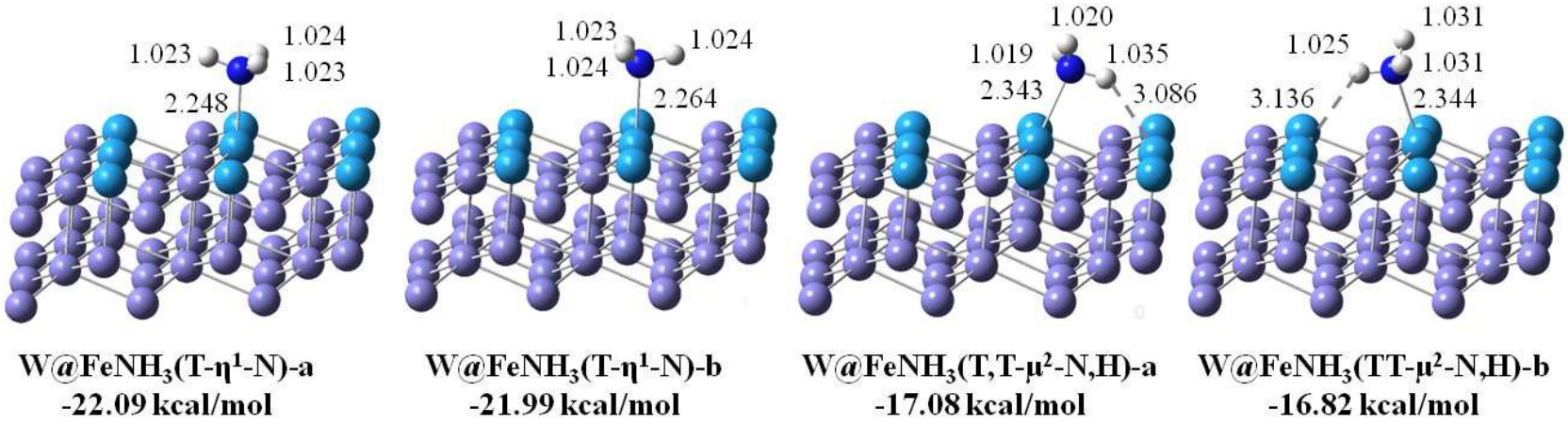

Figure 2.

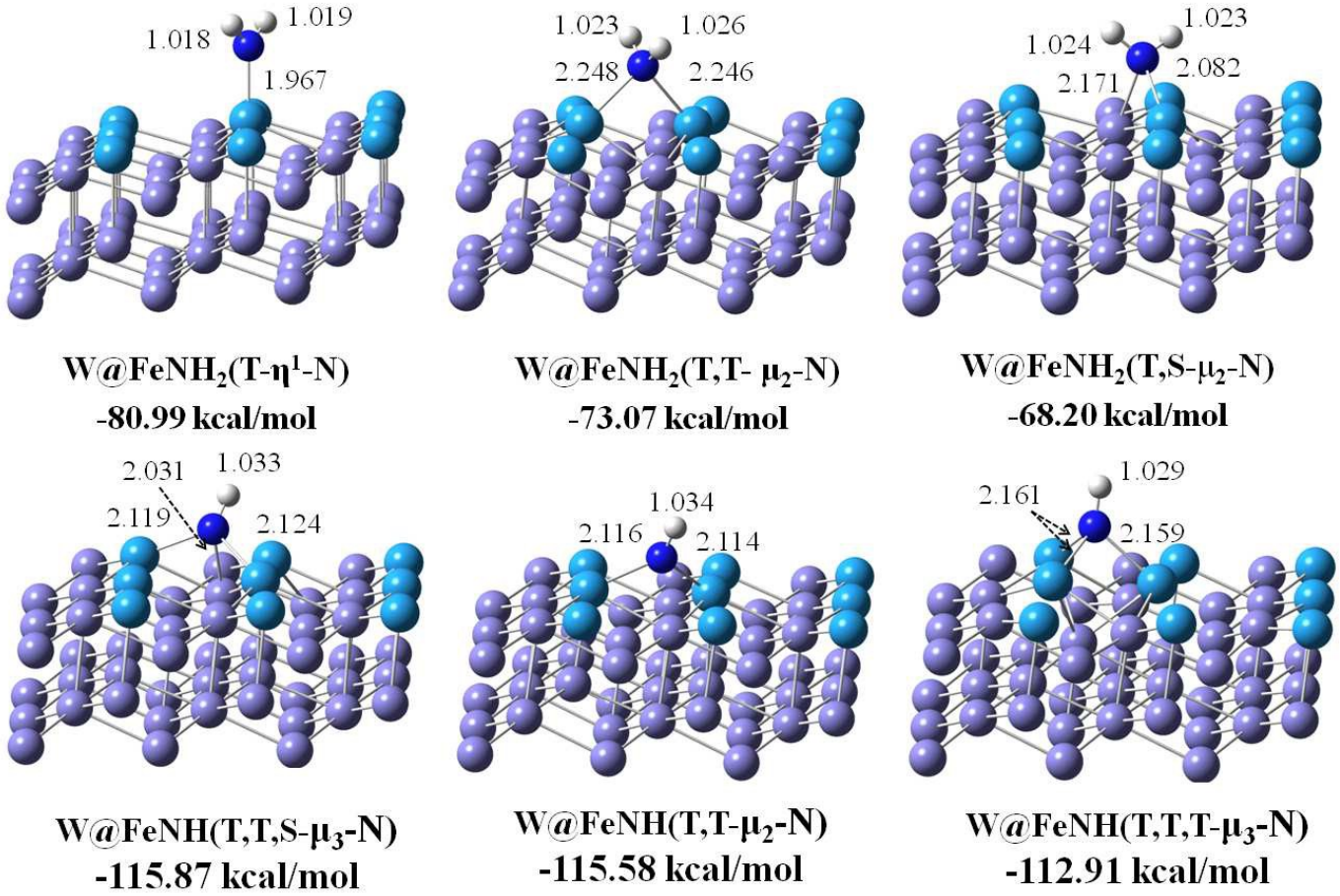

Figure 3.

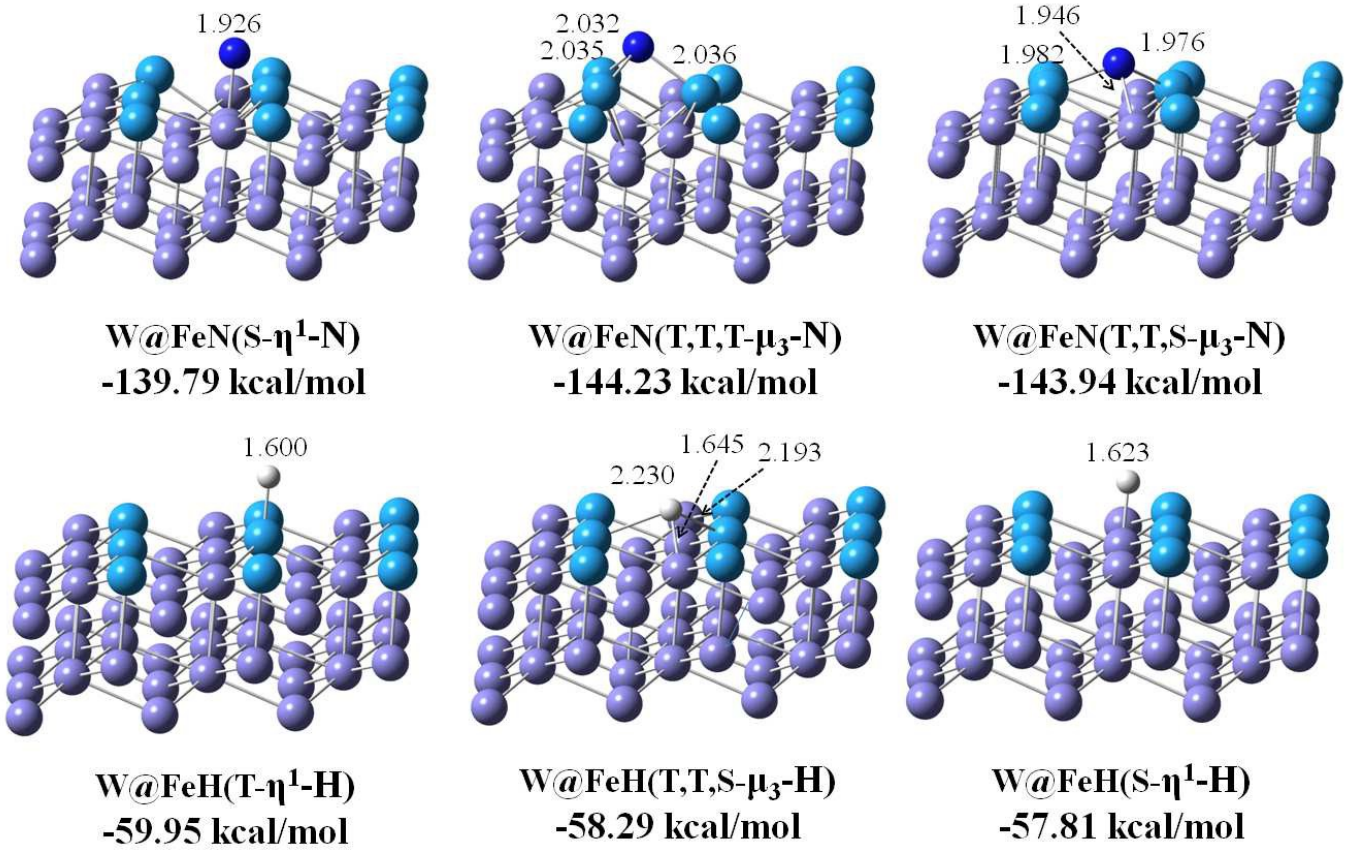

Figure 4.

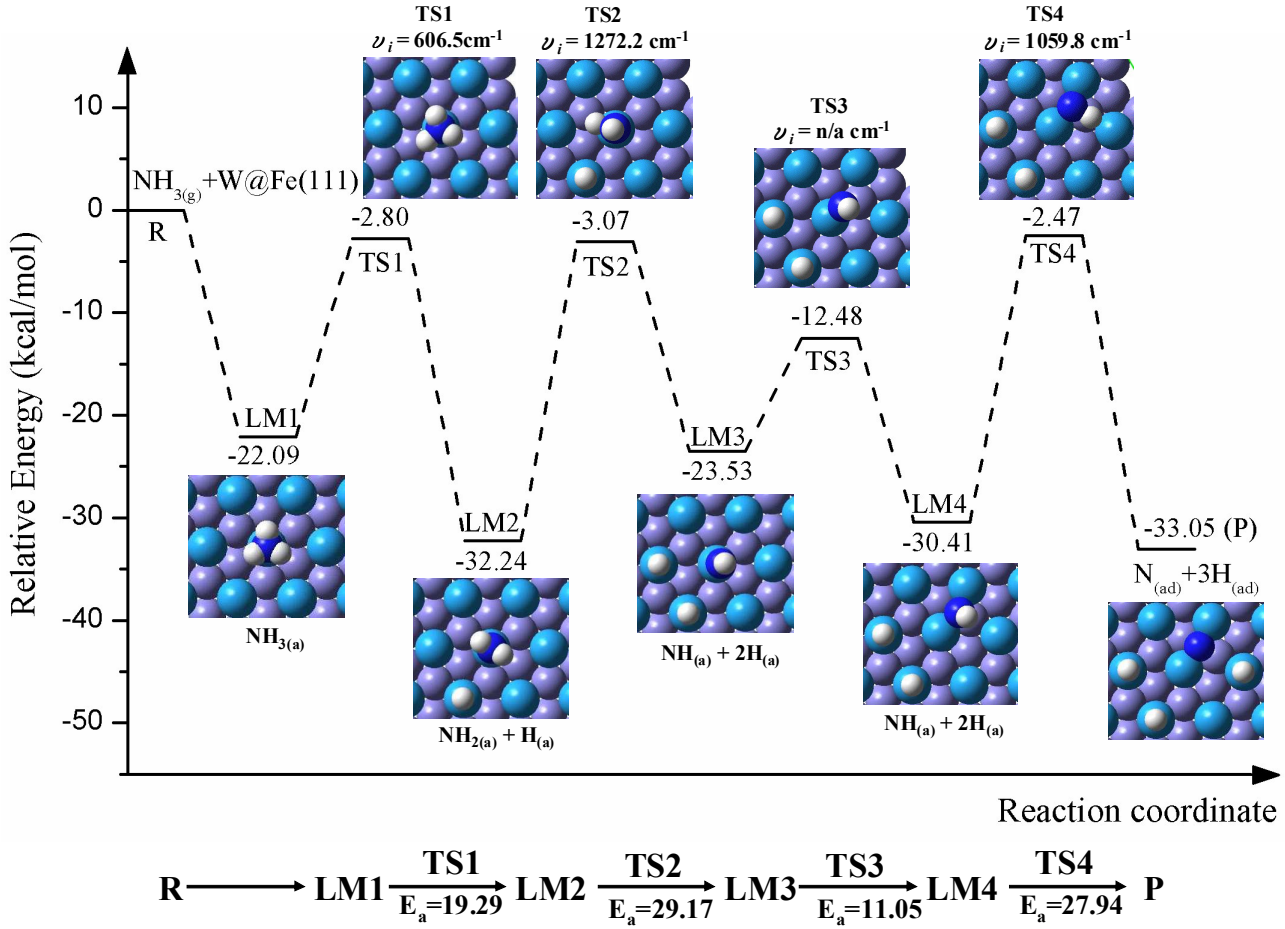

Figure 5.

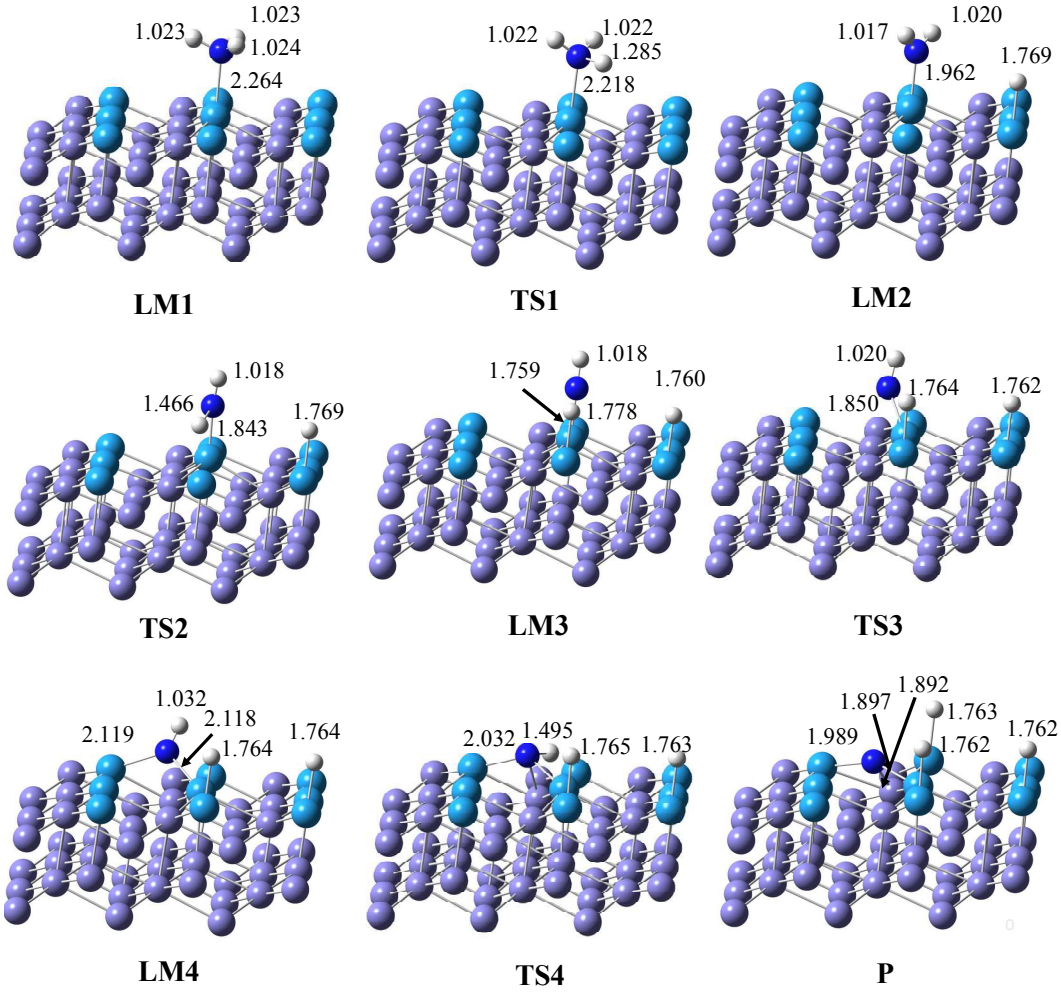

Figure 6.

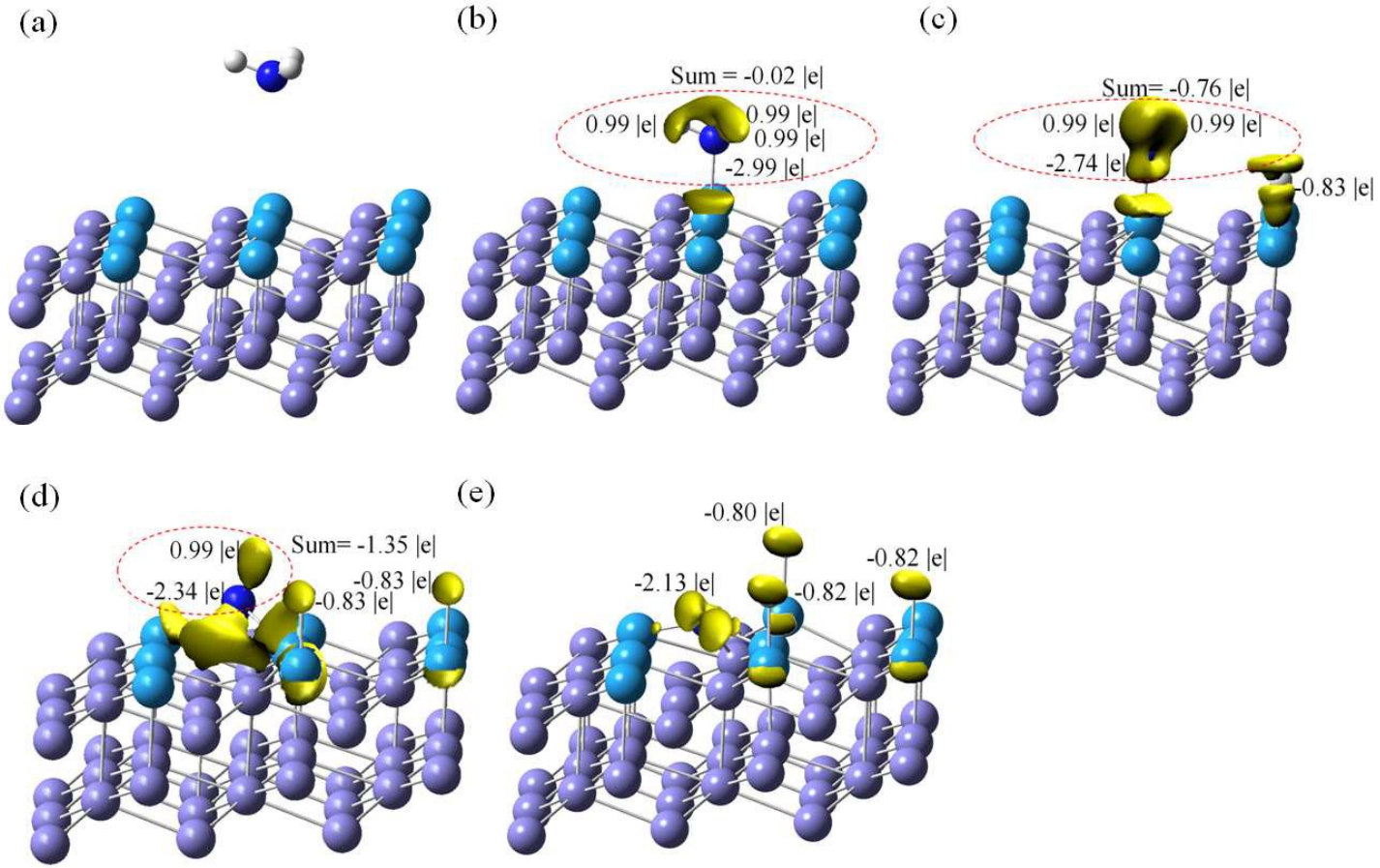

Figure 7.

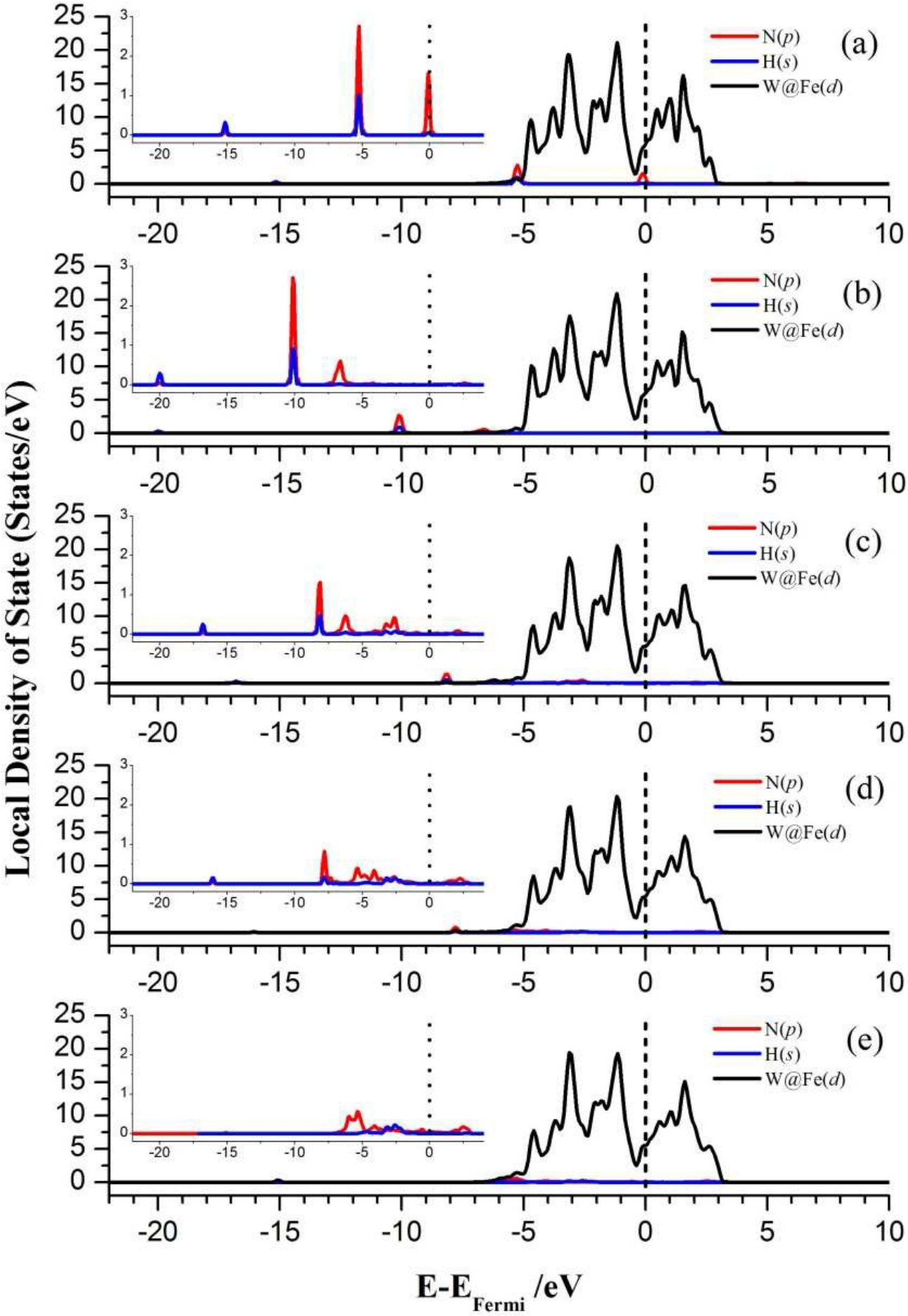

Figure 8.

Table of contents graphic: